Single-Electron Device Simulation

Andreas Scholze, A. Schenk, and Wolfgang Fichtner, *Fellow, IEEE*

Abstract—A three-dimensional (3-D) simulator is presented which uses a linear-response approach to simulate the conductance of semiconductor single-electron transistors at the solid-state level. The many-particle groundstate of the quantum dot, weakly connected to the drain and the source reservoir, is evaluated in a self-consistent manner including quantum-mechanical many-body interactions. A transfer-Hamiltonian approach is used to compute the tunneling rates for the coupling of the quantum dot levels to the macroscopic reservoirs on the basis of realistic barrier potentials. The simulator was applied to a GaAs/AlGaAs example structure. We discuss the conductance characteristic and the capacitances as well as the microscopic structure of the quantum dot.

Index Terms—Coulomb blockade, numerical modeling, single-charge tunneling, single-electron transistors, transfer-Hamiltonian formalism.

I. INTRODUCTION

SINCE the 1980s, developments in both semiconductor technology and theory have led to a completely new field of device research focusing on structures whose operation is based on the discrete nature of electrons tunneling through thin potential barriers. These devices are referred to as *single-electron devices*. The potential of the single-electron concept is rather breathtaking. In principle, it should be possible to operate in the limit of one transferred carrier per bit, the ultimate limit of semiconductor based logic. However, it was not before the mid-1980s that lithography technology reached the deep submicron range making structuring of <100 nm features possible. In the meantime, single-electronics has much matured and a variety of concepts and device architectures are explored.

From the very beginning of semiconductor technology, it was thought that numerical, physics-based analysis of devices could help a great deal in their understanding. Nowadays, simulation and modeling of semiconductor devices both at the process and the device level has become one of the most important development methodologies in industry and research alike. Simulation of single-electron devices, however, is a field still in its infancy. Most of the approaches used today are based on circuit analysis of equivalence circuits containing tunneling junctions and islands characterized by capacitances. All these methods use the results of the phenomenological *orthodox theory* (see for instance, [1]) which treats single-electron transitions between purely capacitively coupled islands (metallic grains) [2], [3]. The advantage of these methods is the possibility to evaluate complex circuits containing a multitude of islands and tunneling junctions. Most of the time, analytical capacitance results are used which retain the simplicity needed for the numerical evaluation of large circuits.

For semiconductor structures, however, the above-mentioned methods are not accurate enough, especially if a discrete energy spectrum is present at the island. An accurate description of the island potential is only possible employing self-consistent methods based on *density-functional theory* (DFT). Here, the device is modeled and simulated at the solid-state level, i.e., the screening of the carriers is included by solving a nonlinear (Schrödinger–) Poisson equation for a realistic geometry. This method allows for a detailed analysis of single-electron charging as for instance the calculation of the exact peak heights of the Coulomb-blockade peaks and of possible envelope modulations.

In this paper, we present a device simulator especially devised for the simulation of single-electron transistors (SETs). It solves the equations relevant for the many-particle groundstate in a quantum dot weakly coupled to two reservoirs by thin tunneling barriers. Quantum-mechanical many-body interactions for the quantum-dot electrons are considered as well as the tunneling from the localized states in the reservoir to the lead contacts. The simulator can handle devices of almost arbitrary shape based on Si and GaAs/AlGaAs. A new numerical scheme has been developed that allows the inclusion of quantum-well, quantum-wire, and quantum-dot-like confinement at the same time and in different regions of the device. The linear-response conductance is calculated on the basis of a free-energy minimization algorithm especially suitable for small quantum dots with strong electron-electron interaction. The simulation results are used to extract macroscopic parameters of the device such as the gate-capacitance and the dot self-capacitance. At the same time, it is possible to study the device on the microscopic level of the wavefunctions and the discrete eigenenergy spectrum.

This paper is organized as follows. In Section II, an extensive discussion of the simulation method is presented. Section III shows the simulation results for a GaAs/AlGaAs based example structure. A comparison with the measured data available for the simulated structure is given. Some conclusions are drawn in Section IV.

II. SIMULATION METHOD

A. Linear-Response Model

The model for a single-electron transistor consists of a confinement region (island, quantum dot) with a discrete level spectrum ε_i $(i = 0, 1, \ldots)$. The occupation of the levels is described by an integer number $n_i = 0, 1$ and the occupation of the level system, i.e., a specific occupation number configuration is given by the set $\{n_i\}$. The number of electrons N is integer and $N = \sum_i n_i$. The confined region is weakly coupled to two electron reservoirs via tunneling barriers (junctions). The reservoirs

which are named *source* and *drain* are taken to be in thermal equilibrium at temperature T and Fermi energy E_F. The device is considered to be driven in linear-response, i.e., the conductance G is defined as $G \equiv I/V$ in the limit $V \to 0$. At $T = 0$ K a current flows if the Fermi energy in the reservoirs aligns with one of the chemical potentials $\mu(N)$ of the quantum dot. The set of chemical potentials $\{\mu(N)\}$ is given as the change in the free energies of the system when adding or removing an electron, i.e., $\mu(N) \equiv F(N) - F(N-1)$. The tunneling through the two barriers is described by sets of tunneling rates for all states k in the quantum dot to the left (drain-) and the right (source-) reservoir, $\{\Gamma_k^d\}$ and $\{\Gamma_k^s\}$. The intrinsic width of the transmission resonance is $\hbar\Gamma_t = \hbar(\Gamma^s + \Gamma^d)$. It is assumed that for all levels in the dot $k_BT \gg \hbar\Gamma_t$, i.e., the finite width of the transmission resonance through the quantum dot can be disregarded. It is further assumed that the junction resistances are above the quasiclassical limit, $R_t \gg R_Q = \hbar\pi/2e^2 \simeq 6.4$ kΩ. This ensures that the tunneling events are well separated in time and the current flow does not disturb the equilibrium. It is therefore possible to use a master equation to describe the transport [4]. Linearization of this master equation leads to an equation for the linear response conductance [5]:

$$G = \frac{e^2}{k_BT} \sum_k \sum_{\{n_i\}} \frac{\Gamma_k^s \Gamma_k^d}{\Gamma_k^s + \Gamma_k^d} P_{\text{eq}}(\{n_i\}) \delta_{n_k,0} f(\epsilon) \qquad (1)$$

where $\epsilon = F(\{n_i\}, n_k = 1, N+1) - F(\{n_i\}, n_k = 0, N) - E_F$. The free energy of the system with the quantum dot in a particular occupation configuration $\{n_i\}$ and electron number N is denoted $F(\{n_i\}, N)$. We use the following notation for the free energies in (1): $F(\{n_i\}, n_k = 1, N+1)$ denotes the free energy of the system with a set of occupation numbers $\{n_i\}$, electron number $N+1$, and the kth level filled, i.e.,

$$F(\{n_i\}, n_k = 1, N+1)$$
$$\equiv F(n_1, \ldots, n_{k-1}, 1, n_{k+1}, \ldots; N+1). \qquad (2)$$

The kth level is assumed empty before the transition from the N-electron system to the $(N+1)$-electron system, and consequently, the free energy associated with the system before charging the quantum dot, $F(\{n_i\}, n_k = 0, N)$, is defined according to

$$F(\{n_i\}, n_k = 0, N)$$
$$\equiv F(n_1, \ldots, n_{k-1}, 0, n_{k+1}, \ldots; N). \qquad (3)$$

The equilibrium distribution function of the grand canonical ensemble, $P_{\text{eq}}(\{n_i\})$, is given by

$$P_{\text{eq}}(\{n_i\}) = \frac{\exp\{-\beta[F(\{n_i\}, N) - E_F N]\}}{\sum_{\{n_j\}} \exp\{-\beta[F(\{n_j\}, N) - E_F N]\}} \qquad (4)$$

with $\beta = (k_BT)^{-1}$, the inverse of the thermal energy.

B. Free Energy Minimization

To calculate the total (Helmholtz) free energy of a charged system consisting of $i = 1 \ldots M$ distinct elements with the

total equilibrium charges Q_i and the voltages V_i the following semi-classical expression is used

$$F = \frac{1}{2} \sum_{i=1}^{M} Q_i V_i - \sum_{i=1}^{M} \int_0^t dt' I_i(t') V_i(t') \qquad (5)$$

where I_i denotes the currents provided by the external circuitry (voltage sources). The first term in (5) is the capacitive (potential-) energy U stored in the device. Separating the device into elements that contain a continuous space charge ρ (dot, leads, donor layer) and metal plates which are equipotential regions (gates, contacts) the electrostatic energy U can be separated into

$$U = \frac{1}{2} \int_{\hat{\Omega}} d\mathbf{r}\, \rho(\mathbf{r})\phi(\mathbf{r}) + \frac{1}{2} \sum_{i \in \text{gates}} Q_i V_i. \qquad (6)$$

The potential ϕ is the electrostatic potential, i.e., the solution of the Poisson equation with the charge density ρ subject to boundary conditions at the gates and contacts. The integral over the space charges replaces the summation over the M charged elements in (5). The energy contribution from the gates, which are kept at constant voltages V_i, is calculated with the surface charges Q_i. The second term in (5) is the work W which is needed to charge all elements that are connected to external circuitry (such as the gates and the source and drain region) when N electrons are transferred to the quantum dot region. It is assumed that the charging is fast compared with the internal relaxation times, i.e., the tunneling time τ. Voltage sources are considered to be ideal with zero internal resistances (low-impedance environment). Therefore, it is reasonable to assume that the voltages are kept at constant level before and after the charging $V_i(t) = V_i(0)$. Using $I = dQ/dt$ the current integral in (5), i.e., the work W_i for the charging of the ith element, is written

$$W_i = V_i \int_0^t dt' I_i(t') = V_i[Q_i(t) - Q_i(0)] = V_i Q_i \qquad (7)$$

where the number of electrons in the dot at time zero is arbitrarily set to zero. At time t the dot contains N electrons. The final form of the semiclassical Helmholtz free energy is therefore given as

$$F = \frac{1}{2} \sum_{\substack{i \notin \text{leads} \\ \text{gates}}} \int_{\hat{\Omega}_i} d\mathbf{r}\, \rho(\mathbf{r})\phi(\mathbf{r})$$
$$- \frac{1}{2} \sum_{i \in \text{leads}} \int_{\hat{\Omega}_i} d\mathbf{r}\, \rho(\mathbf{r})\phi(\mathbf{r})$$
$$- \frac{1}{2} \sum_{i \in \text{gates}} Q_i V_i. \qquad (8)$$

In the case of bound states in a zero-dimensional electron gas, the free energy has to be modified including the influence of the confined states on the total energy of the quantum dot [7], [8]. The Helmholtz free energy, (5), is extended by two terms, i.e.,

$$F(\{n_k\}, N) = \sum_k n_k \varepsilon_k^0 + E_{\text{xc}} + \frac{1}{2} \sum_{i=1}^{M} Q_i V_i$$
$$- \sum_{i=1}^{M} \int_0^t dt' I_i(t') V_i(t'). \qquad (9)$$

The first sum over the bare (noninteracting) dot levels ε_k^0 with a particular occupation configuration $\{n_k\}$ is the interaction-free kinetic energy of the quantum dot T_s. We use a parameterized form of the exchange-correlation energy of the electrons, E_{xc}, which corresponds to a local exchange-correlation potential V_{xc} [6]. The total energy contribution of the quantum dot electrons to the Helmholtz free energy in (9) is

$$
\begin{aligned}
E_{\mathrm{tot}}&(\{n_k\}, Q_{\mathrm{dot}}, V_{\mathrm{dot}}) \\
&= \sum_k n_k \varepsilon_k^0 + \frac{1}{2} Q_{\mathrm{dot}} V_{\mathrm{dot}} + E_{\mathrm{xc}}.
\end{aligned}
\tag{10}
$$

The self-consistent single-particle energies ε_k are calculated solving a three-dimensional (3-D) Kohn–Sham equation with the effective potential $\mathcal{V}_{\mathrm{eff}}(\mathbf{r}) = \Delta E_c(\mathbf{r}) - q\phi(\mathbf{r}) + V_{\mathrm{xc}}(\mathbf{r})$ where ΔE_c is the conduction-band offset. This leads to the following form for the ε_k:

$$
\varepsilon_k = \varepsilon_k^0 + \langle \psi_k | - q\phi(\mathbf{r}) | \psi_k \rangle + \langle \psi_k | V_{\mathrm{xc}}(\mathbf{r}) | \psi_k \rangle.
\tag{11}
$$

Small thermal variations in the level occupancies have a negligible effect on the self-consistent results (ε_k, ϕ, ρ, and Q_i) which are implicit functions of the electron number and the applied voltages. This is especially true at low temperatures where the level spacing is hardly affected by the temperature. Therefore, the occupation configuration dependence of the last two terms is ignored and the discrete occupation numbers n_k are replaced by the noninteger occupation numbers according to the Fermi–Dirac distribution [7]. With this approximation, the interaction-free kinetic energy is obtained as

$$
\begin{aligned}
T_s(\{n_k\}) = &\sum_k n_k \varepsilon_k \\
&+ q \int_\Omega d\mathbf{r}\, n(\mathbf{r})\phi(\mathbf{r}) - \int_\Omega d\mathbf{r}\, n(\mathbf{r}) V_{\mathrm{xc}}(\mathbf{r}).
\end{aligned}
\tag{12}
$$

The above result is inserted into (10), where the electrostatic energy is replaced according to

$$
\frac{1}{2} Q_{\mathrm{dot}} V_{\mathrm{dot}} \rightarrow -\frac{1}{2} q \int_\Omega d\mathbf{r}\, n(\mathbf{r})\phi(\mathbf{r}).
\tag{13}
$$

The final expression for E_{tot} becomes

$$
\begin{aligned}
E_{\mathrm{tot}}&(\{n_k\}, \rho, \phi) \\
&= \sum_k n_k \varepsilon_k + \frac{1}{2} q \int_\Omega d\mathbf{r}\, n(\mathbf{r})\phi(\mathbf{r}) \\
&\quad + E_{\mathrm{xc}} - \int_\Omega d\mathbf{r}\, n(\mathbf{r}) V_{\mathrm{xc}}(\mathbf{r}).
\end{aligned}
\tag{14}
$$

The integration is over the quantum dot area Ω only and the electron density n is always positive. The total energy of the quantum dot, E_{tot}, is included in the Helmholtz free energy given by (9). This leads to the final form of the free energy $F(\{n_k\}, N)$.

In the following, the method used in the simulator to minimize the free energy is discussed. The chemical potential μ of the quantum dot is ramped and the self-consistent ground states
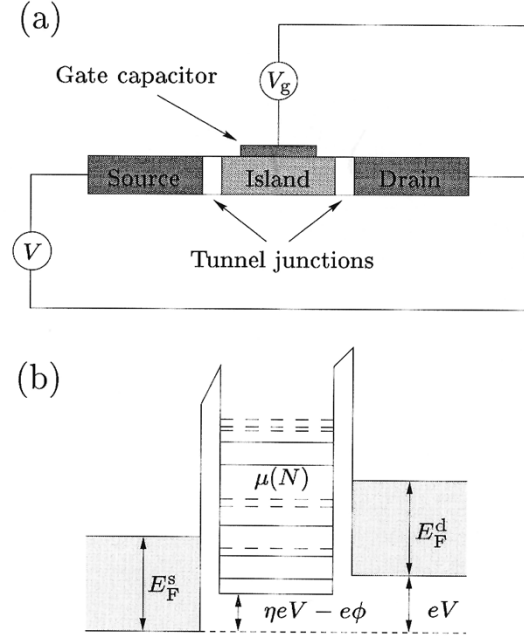
Fig. 1. (a) Schematic drawing of a SET. (b) Potential cut through the structure. Electrons in the island occupy discrete levels (long dashed lines). The chemical potentials $\mu(N)$ according to discrete numbers of electrons are indicated by straight lines.

and the free energies are calculated using the equations from the previous section for $5 \ldots 7$ sample points of μ. The free energies form a parabola if plotted as a function of the chemical potential. The number of electrons in the quantum dot is noninteger in general, since we use arbitrary values for μ. However, as already stated in Section II.A, the chemical potentials $\mu = \mu(N)$ form a discrete set and are only allowed for integer numbers of N (c.f. Fig. 1). Therefore, the free energies $F(\{n_k\}, N)$ (for integer values of N) are determined by spline interpolation using the free energy values already calculated at the sample points. These free energy values are used in the Gibbs distribution, (4), to calculate the equilibrium number of electrons in the dot and the conductance according to (1).

C. Tunneling Theory

We use the *transfer Hamiltonian* formalism introduced by Bardeen [9] to calculate the tunneling rates Γ_p between a reservoir and the quantum dot. The quantum dot is separated from the reservoir by a narrow quasi-one-dimensional (qwasi–1-D) channel. By applying a voltage to an electrostatic gate above the channel a narrow constriction is created (see Fig. 2). Since the constriction is formed electrostatically, its boundaries are smooth and electron scattering can be neglected. An ideal quantum point contact (QPC) is formed.

The wavefunction inside the constriction is one-dimensional. The width of the constriction can not be considered constant, however. The simplest theory for this case is based on the *adiabatic approximation*, which assumes that the cross section of the channel changes so slowly that there is only negligible scattering between the subbands. Transport is possible only in the x-direction and confinement of carriers occurs in the yz-plane.
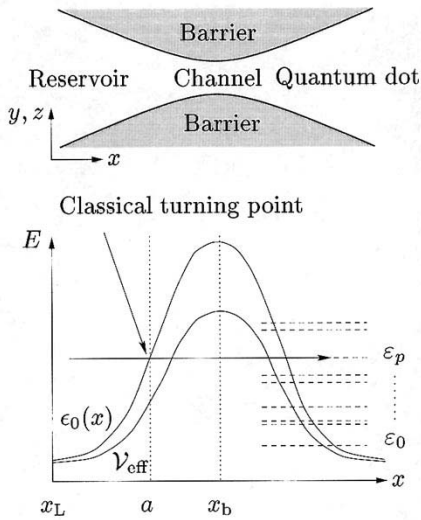
Fig. 2. (a) Schematic view of the constriction. (b) The barrier potential, the energies of the lowest subband and the quantum dot spectrum. a is the classical turning point in the reservoir.

At each value of x along the channel a two-dimensional (2-D) Schrödinger equation

$$\left[-\frac{\hbar^2}{2m_\perp^*} \left(\frac{\partial^2}{\partial y^2} + \frac{\partial^2}{\partial z^2} \right) + \mathcal{V}_{\text{eff}}(x,y,z) - \epsilon_n(x) \right] \phi_n(x;y,z) = 0 \quad (15)$$

for the transverse eigenfunctions $\phi_n(x;y,z)$ and the subband energies $\epsilon_n(x)$ is solved where $m_\perp^*$ is the electron effective mass perpendicular to the transport direction. The full wave function ψ satisfying the three-dimensional (3-D) Schrödinger equation factorizes as

$$\psi \longrightarrow \psi_{nk}(x,y,z) = \phi_n(x;y,z)\xi_k(x) \quad (16)$$

where the $\xi_k(x)$ are the solutions to the coupled-mode equation

$$\left[-\frac{\hbar^2}{2m_\parallel^*} \frac{\partial^2}{\partial x^2} + \epsilon_n(x) \right] \xi_k(x) = E_{nk}\xi_k(x). \quad (17)$$

The total energy is

$$E \longrightarrow E_{nk} = \epsilon_n(x) + \frac{\hbar^2 k^2}{2m_\parallel^*}. \quad (18)$$

Now, the case of an electron moving from a reservoir state labeled E_{nk} to a zero-dimensional quantum-dot state ε_p is considered. Energy conservation in the tunneling process requires that $E_{nk} = \varepsilon_p$. It is convenient to assume that $\mathcal{V}_{\text{eff}}$ is constant outside a larger range to the left-hand side of the barrier $x < x_L$, i.e., $\epsilon_n(x) = \mathcal{V}_{\text{eff},L} = \text{const}$ for $x < x_L \leq a$ (see Fig. 2). Since the constriction is formed electrostatically, its boundaries are smooth and scattered components $(\exp(-ikx))$ of the wavefunction can be neglected. The *classical turning point* in the reservoir a is the point in x where $E_{nk} = \varepsilon_p$, i.e., where the energies of the electron before and after the tunneling process are matched and the *classically forbidden* region starts. Classically, the wave is reflected at this point. Quantum mechanically,

it can tunnel through the barrier. The WKB approximation is used in the forbidden region $x > a$. The wave function component in x is

$$\xi_\kappa(x) = \exp[w(x)] \quad \text{with}$$
$$w(x) = \int_a^x dx' \, \kappa(x') \quad (19)$$

and $\kappa(x)$ is the positive root

$$\frac{\hbar^2}{2m_\parallel^*}\kappa^2(x) = \epsilon_n(x) - E_{nk} \quad (20)$$

with the assumption of $|d\kappa/dx| \ll \kappa^2$. The constriction is assumed narrow enough that only a single transverse state is below the Fermi level. As the electron moves away from the constriction, the channel becomes wider and the number of transverse states grows. However, within the constriction a single mode is present, i.e., the matrix element is calculated only for the transition from the ground state $(n = 0)$. Both the channel region and the quantum dot region overlap and the matrix element is calculated by integrating over a surface $\partial\Omega$ in the yz-plane at some point x_b (usually taken as the mid-point of the barrier). This leads to

$$M_p \approx -\frac{\hbar^2}{2m_\perp^*}\xi_\kappa(x_b) \iint\limits_{\partial\Omega(y,z)} dy\,dz\,\phi_0(x_b;y,z)$$
$$\times \left[\kappa(x_b)\psi_p(x_b;y,z) - \frac{\partial}{\partial x}\psi_p(x_b;y,z) \right] \quad (21)$$

where $\kappa(x_b)$ is defined by (20) with $E_{0k} = \varepsilon_p$. The transition rate for the tunneling from the lowest reservoir subband to the pth quantum dot state, Γ_p, is obtained from Fermi's golden rule, i.e.,

$$\Gamma_p = \frac{2\pi}{\hbar}|M_p|^2. \quad (22)$$

III. SIMULATION EXAMPLES

The example device investigated here is shown in Fig. 3. The 3-D structure is mapped onto a three dimensional nonuniform tensor-product grid with $69 \times 36 \times 70$ grid points along $x \times y \times z$ comprising a total of 173 880 vertex nodes. The total area simulated is a bricklike region of $1000\,\text{nm} \times 600\,\text{nm} \times 290\,\text{nm}$. The substrate, which is extending 2.8 μm in the negative z-direction is effectively cut-off at 290 nm imposing von Neumann boundary conditions at this surface as well as at the surfaces in the lateral xy-directions where the electric field vanishes at distances far enough from the active device region. The Fermi level in the substrate is set assuming an electrode outside the simulated region. Part of the top surface of the device is covered by metal gates for which Dirichlet boundary conditions for Schottky contacts are employed. The Schottky barrier is set to $\phi_s = 800$ meV. The rest is exposed GaAs. Since the exposed surface covers a substantial portion of the surface, the choice of the appropriate boundary condition is crucial for the determination of the electrostatic potential in the whole device. The properties of exposed GaAs surfaces are dominated by a band of surface states near the middle of the band gap. While the states underneath the metal gate can be
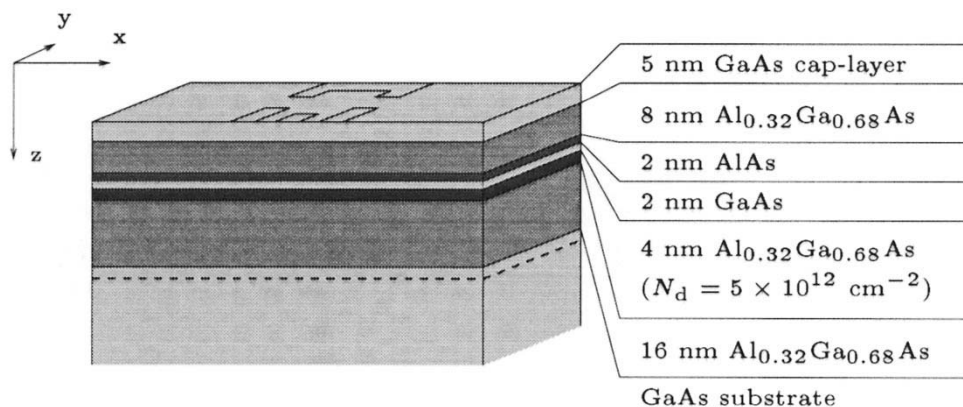
Fig. 3. Schematic of the horizontal structure of the GaAs/AlGaAs heterostructure. The dashed line marks the 2-DEG.
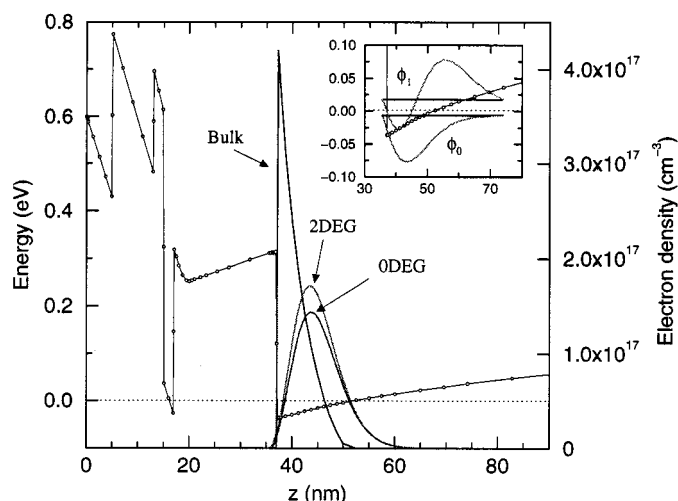
Fig. 4. Conduction-band edge and electron densities along the z-direction at 1 K. The circles at the conduction-band curve show the position of the grid planes in xy-direction. The inset displays the wavefunctions of the first two subbands corresponding to the 2-DEG model.

Fig. 5. Split-gate structure (top), electron density (middle) and conduction-band edge (bottom) in a lateral xy-plane. The density and band-edge cuts are taken 8 nm below the GaAs/AlGaAs heterojunction in the 0-DEG/2-DEG. The control-gate voltage V_g is applied at the gate asterisked **C**.

assumed to be pinned to the metal Fermi level, those at the exposed surface are assumed to be pinned at the substrate Fermi level. *Fermi-level pinning* is modeled using Dirichlet boundary conditions for the electrostatic potential at the surface and a pinning value of $\phi_{\mathrm{pin}} = 600 \, \mathrm{meV}$.

Fig. 4 shows the conduction-band edge and the electron densities along the z-direction. Displayed are the densities for a parabolic-band model (Bulk), a 2-D electron-gas model (2-DEG), and a zero-dimensional electron-gas model (0-DEG). Only the lowest subband is occupied in the 2DEG model. The subband energies ϕ_1 and ϕ_2 are 31 meV and 55 meV above the conduction-band edge at the GaAs/AlGaAs heterojunction and the difference of the Fermi energy to the lowest subband is 6 meV. The conduction-band edge and the electron-charge density in the lateral xy-plane is shown in Fig. 5. The electron density in the center (quantum dot) was calculated using a 0DEG model, i.e., solving a 3-D-Schrödinger equation. The distorted shape of the quantum dot potential is reflected in the shape of the individual wavefunctions (Fig. 6). One observes a tendency to form

quasi-1-D wavefunction-*scars*. These scars are related to the classical trajectories of particles entering the dot, then bouncing within, and finally exiting. The occurrence of scars is an indication that the quantum dot is already acquiring properties of a disordered ballistic structure in which conductance fluctuations can be understood as interference of phase-coherent electrons traversing the dot via a number of distinct classical paths. Two pronounced families of scars are visible in Fig. 6. The first family (S1) is related to the wavefunctions labeled 4, 6, 9, 12, 15, 19, 23, 28, 33 and the second (S2) to 5, 8, 11, 16, 20, 26, 31.

Fig. 7 shows the tunneling rates versus the eigenenergies at a particular value of the gate voltage ($V_g = -400 \, \mathrm{meV}$) calculated using the wavefunctions in Fig. 6. The tunneling rates belonging to one particular scar family are linked by dotted lines. It can be seen that especially the rates related to S1 have almost the same value which can be explained by the similar shape of the wavefunctions, leading to similar values for the overlap integral between the lead and the quantum dot wavefunction. The highest values, however, are related to the wavefunctions which are more uniformly distributed over the
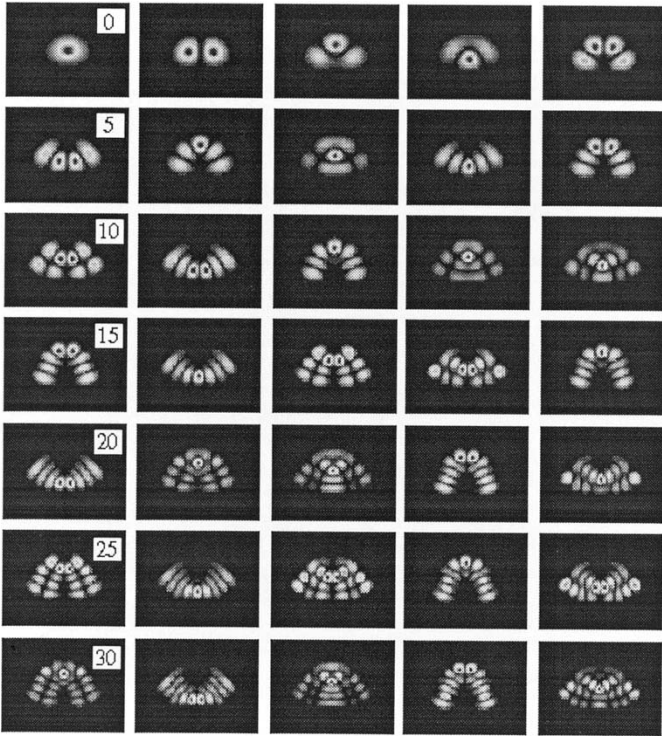
Fig. 6. Single-particle levels ($|\psi_i|^2$, $i = 0 \ldots 34$; spin-degenerate). The cut has been taken in the xy-plane 8 nm below the GaAs/AlGaAs interface in the 0-DEG. The lead channels are situated to the left and the right of each individual plot.

quantum dot area, showing some alignment along the x-axis (see for example states 24, 29, and 35 in Fig. 6).

We use the doping density in the doping sheet as a parameter to adjust the number of electrons in the quantum dot to a particular range. The lower panel of Fig. 8 shows the conductance characteristics for the low-filling regime where the number of electrons increases from 49 to 66, whereas the upper panel shows the conductance in the high-filling regime where the number of electrons increases from 88 to 110. The overall values of the conductance become larger with increasing electron number. The reason for this is the lateral extension of the 0-DEG and the consequently smaller barrier thicknesses when the dot is filled with more and more electrons. The electron-wavefunction coupling to the leads is stronger and this results in higher tunneling rates. In fact, the peak values in the upper panel almost exceed the maximal allowed value of $G_Q = 4e^2/h$, i.e., the limit for the applicability of (1) is clearly reached.

The envelopes of the conductance peaks exhibit some modulations that are more pronounced for lower temperatures. These modulations are due to coherent-resonant transport through the quantum dot rather than due to shell-filling effects. The quantum dot is acting as a resonator, and the electrons are reflected by the quantum point contacts similar to a Fabry–Perot interferometer. A quantum-mechanical interpretation can be given: those states which are more situated in the center of the quantum dot, showing some alignment with the x-direction, contribute the most to the transport by being related to the highest tunneling rates. Strong coupling can be observed, for example, for the states labeled 24, 29, and 35 (Fig. 7). If one takes the twofold
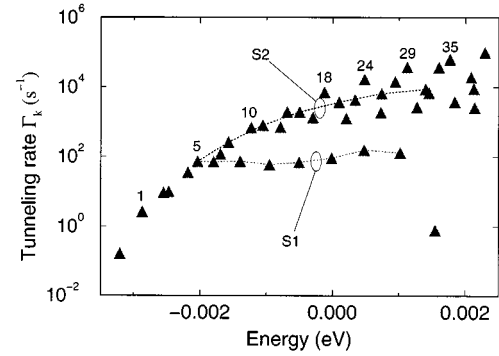
Fig. 7. Tunneling rates, i.e., elastic couplings of the dot wavefunctions to the leads versus the single-particle eigenenergies. The dotted lines link the rates that belong to one of the scar families (S1 and S2).
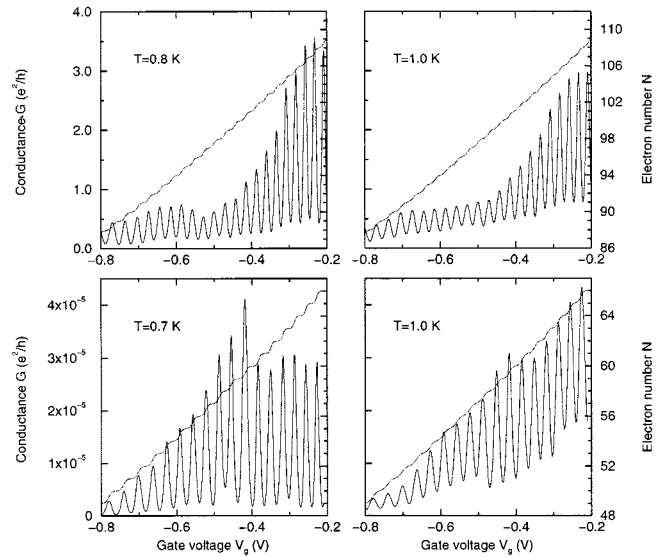
Fig. 8. Electron charging N and conductance G in units of the conductance quantum e^2/h versus the gate voltage V_g at different temperatures. The lower panel shows the low-filling regime ($N = 49 \ldots 66$) and the upper panel the high-filling regime ($N = 88 \ldots 110$).

spin-degeneracy of the states into account, the maximum of the envelope of the $T = 0.7$ K conductance curve (Fig. 8), for instance, can be attributed to the filling of state 29, i.e., the charging of the quantum dot from 59 to 60 electrons.

The gate capacitance C_g, i.e., the capacitive coupling of the control gate to the quantum dot may be defined as

$$C_g = \frac{dQ}{dV_g} \tag{23}$$

where Q is the quantum dot charge. Therefore, the gate capacitance is calculated by numerically differentiating the Coulomb-staircase (Fig. 9). Another method to evaluate the gate capacitance is via the spacing of the Coulomb-blockade peaks. The difference ΔV_g between the Nth and the $(N+1)$th peak is used and the gate capacitance is calculated as

$$C_g(N) = \frac{e}{\Delta V_g} = \frac{e}{V_g(N+1) - V_g(N)}. \tag{24}$$

The capacitance is now a function of N (Fig. 10). Both methods give similar results for the gate capacitance which increases from 5 aF to a value of around 7 aF over the range of the conductance calculations.

The concept of self-capacitance for a semiconductor quantum dot is difficult since the dimensions of the dot are comparable with the screening length and the voltage is not specified by a single number. One possible definition, which is still meaningful, is based on differential capacitances [10]. A self-capacitance C_{dd} is defined as the amount of work, ΔV, to bring fixed amount of charge, ΔQ, to the quantum dot, i.e., $e\Delta V = \mu(N + \Delta N) - \mu(N)$ and $\mu(N)$ is the chemical potential of the N-particle system. The capacitance can be written as

$$\frac{e^2}{C_{\mathrm{dd}}(N)} = \mu(N+1) - \mu(N). \tag{25}$$

The quantum dot self-capacitance $C_{\mathrm{dd}}(N)$ (Fig. 11) was calculated using the self-consistent structure results. The quantum dot chemical potential was extracted from the free energy minimization. The zig-zag shape of the capacitance curve is due to even-odd level filling of the spin-degenerate single-particle levels in the quantum dot.

Conductance measurements for a similar structure to the one used here can be found in [11]. The main difference to the experimental results is the much larger period of the conductance oscillations. This corresponds to a much higher measured gate capacitance of 32 aF. A possible reason for this discrepancy is the assumption of Fermi-level pinning for the exposed parts of the GaAs surface. This means that only the potential at the control gate C moves with the changing gate voltage. However, calculations by Laux *et al.*[12] for a similar GaAs/AlGaAs heterostructure using a drift-diffusion simulator and allowing the surface states to equilibrate with the gate show that the exposed surface immediately surrounding the gate would effectively become part of it. The increased effective size of the gate leads to an increased capacitance. This allows us to conclude that the equilibrium approach proposed here is always bound to underestimate the coupling capacitances between the gates and the quantum dot, even though it is difficult at this point to give a more quantitative argument.

IV. Discussion

We showed simulations for a realistic single-electron transistor based on a GaAs/AlGaAs split-gate structure. Main features as the conductance and the capacitances have been computed and the interplay of the microscopic structure of the 0-DEG in the quantum dot and the macroscopic environment has been discussed. Remaining discrepancies as the underestimation of the capacitive coupling of the gates to the quantum dot are probably due to the physical model for the exposed GaAs surface. Additional uncertainty arises from the treatment of the doping sheet. The doping density in the sheet has to be reduced from that grown in the structure since deep levels are neglected. This is reasonable since half of the electrons occupy deep levels. These levels are usually found well below the Fermi-level and the associated charge can be assumed to be frozen out. Furthermore, little is known about the cross section
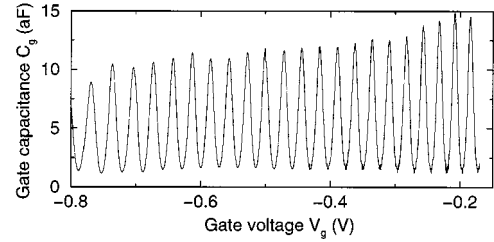
Fig. 9. Gate capacitance C_g from numerically differentiating the Coulomb staircase $N(V_g)$ at $T = 0.8$ K in Fig. 8 (upper panel).
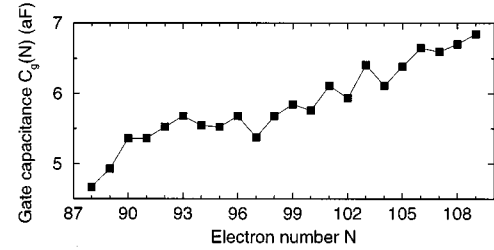
Fig. 10. Gate capacitance C_g as a function of the electron charge N at the dot at $T = 0.8$ K.
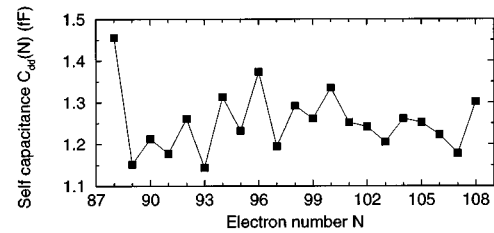
Fig. 11. Quantum dot self-capacitance C_{dd} as a function of the electron number N at the dot at $T = 0.8$ K.

of the doping sheet. Consequently, the exact doping-density distribution is not known. We assume a doping sheet of 2 nm thickness and a constant density of $1\ldots1.5 \times 10^{19}$ cm^{-3}. The remaining uncertainty is used to adjust the number of electrons in the quantum dot within a reasonable range. An improved method, however, should include a more sophisticated treatment of both the exposed surface and the doping sheet in order to get a better description of the electrostatic environment of the quantum dot.

References

[1] K. K. Likharev, "Single-electron devices and their applications," in *Proc. IEEE*, vol. 87, 1999, pp. 606–632.

[2] N. S. Bakhvalov, G. S. Kazacha, K. K. Likharev, and S. I. Serduykova, "Single-electron solitons in one-dimensional tunnel structures," *Sov. Phys.—JETP*, vol. 68, pp. 581–587, 1989.

[3] C. Wasshuber, H. Kosina, and S. Selberherr, "SIMON—A simulator for single-electron tunnel devices and circuits," *IEEE J. Technol. Computer-Aided Design*, vol. 16, pp. 937–944, 1997.

[4] D. V. Averin, A. N. Korotkov, and K. K. Likharev, "Theory of single-electron charging of quantum wells and dots," *Phys. Rev. B*, vol. 44, pp. 6199–6211, 1991.

[5] C. W. J. Beenakker, "Theory of Coulomb-blockade oscillations in the conductance of a quantum dot," *Phys. Rev. B*, vol. 44, pp. 1646–1656, 1991.

[6] J. P. Perdew and A. Zunger, "Self-interaction correction to density-functional approximations for many-electron systems," *Phys. Rev. B*, vol. 23, pp. 5048–5079, 1981.

[7] M. Stopa, Y. Aoyagi, and T. Sugano, "Coulomb oscillation amplitude enhancement and envelope modulation in a magnetic field and activated tunneling," *Surf. Sci.*, vol. 305, pp. 571–575, 1994.

[8] M. Stopa, "Quantum dot self-consistent electronic structure and the Coulomb blockade," *Phys. Rev. B*, vol. 54, pp. 13 767–13 783, 1996.

[9] J. Bardeen, "Tunneling from a many-particle point of view," *Phys. Rev. Lett.*, vol. 6, pp. 57–59, 1961.

[10] G. J. Iafrate, K. Hess, J. B. Krieger, and M. Macucci, "Capacitive nature of atomic-sized structures," *Phys. Rev. B*, vol. 52, pp. 10 737–10 739, 1995.

[11] F. Simmel, T. Heinzel, and D. A. Wharam, "Statistics of conductance oscillations of a quantum dot in the Coulomb-blockade regime," *Europhys. Lett.*, vol. 38, pp. 123–128, 1997.

[12] S. E. Laux, D. J. Frank, and F. Stern, "Quasi-one-dimensional electron states in a split-gate GaAs/AlGaAs heterostructure," *Surf. Sci.*, vol. 196, pp. 101–106, 1988.

A. Schenk was born in Berlin, Germany, in 1957. He received the Dipl. degree in physics and the Ph.D. degree in theoretical physics from the Humboldt University Berlin (HUB), Germany, in 1981 and 1987, respectively.

In 1987, he became a Research Assistant at the Department of Semiconductor Theory, HUB, and in1988 he joined the R&D division of WF Berlin. From 1987 to 1991, he worked on various aspects of the physics and simulation of optoelectronic devices, especially infrared detector arrays and the development and implementation of physical models for modeling infrared sensors. He is now with the Integrated Systems Laboratory, Swiss Federal Institute of Technology, Zurich, Switzerland, as a Senior Lecturer. His main activities are in the development of physics-based models for simulation of submicron silicon devices.

Dr. Schenk is a member of the German Physical Society.

Andreas Scholze was born in 1969. He received the Dipl. Phys. degree from the University of Jena in 1995.

After graduation, he joined the Integrated Systems Laboratory, Swiss Federal Institute of Technology, Zurich, as a Research Assistant, where he now works with the group of Prof. W. Fichtner in the fields of nanodevice simulation and novel device principles. His main activities include the development of device-simulation software for the simulation of nanodevices, especially of single-electron transitors.

Wolfgang Fichtner (M'79–SM'84–F'90) received the Dipl. Ing. degree in physics and the Ph.D. degree in electrical engineering from the Technical University of Vienna (TU), Austria, in 1974 and 1978, respectively.

From 1975 to 1978, he was an Assistant Professor in the Department of Electrical Engineering, TU Vienna. From 1979 to 1985, he was with AT&T Bell Laboratories, Murray Hill, NJ. Since 1985, he has been Professor and Head of the Integrated Systems Laboratory , Swiss Federal Institute of Technology, Zurich. In 1993, he founded ISE Integrated Systems Engineering AG, a company in the field of technology CAD.

Dr. Fichtner is a a member of the Swiss National Academy of Engineering.